



ELSEVIER

Available at www.sciencedirect.com

ScienceDirect

journal homepage: www.elsevier.com/locate/bbe

Original Research Article

Classification of mild and severe adolescent idiopathic scoliosis (AIS) from healthy subjects via a supervised learning model based on electromyogram and ground reaction force data during gait



Arnab Sikidar ^a, Koyyana Eshwar Chandra Vidyasagar ^{a,b}, Manish Gupta ^c, Bhavuk Garg ^c, Dinesh Kalyanasundaram ^{a,d,*}

^a Centre for Biomedical Engineering, Indian Institute of Technology Delhi, New Delhi, India

^b Department of Biomedical Engineering, College of Engineering, Osmania University, Hyderabad, India

^c Department of Orthopedics, All India Institute of Medical Sciences, New Delhi, India

^d Department of Biomedical Engineering, All India Institute of Medical Sciences, New Delhi, India

ARTICLE INFO

Article history:

Received 14 March 2022

Received in revised form

7 June 2022

Accepted 21 June 2022

Available online 01 July 2022

ABSTRACT

At early stages, adolescent idiopathic scoliosis (AIS) is quite hard to be distinguished from healthy (HC) subjects by the naked eye. AIS demands multiple corrective surgeries when detected later, thereby causing significant physical and psychological trauma as no mathematical models exist for the classification of mild AIS (MS) ($20^\circ < \text{Cobb's angle} < 40^\circ$) from HC, we propose a k-nearest neighbour (kNN) method based model. In this work, we collected both the EMG and GRF data from nine severe AIS (SS), three MS and four female HC during gait. Delayed muscle activation in Erector spinae Iliocostalis, Gluteus Medius and Gastrocnemius lateralis was observed in SS compared to HC. However, no such distinction was noticed between MS and HC motivating for a mathematical model. Eighteen time-domain and nine frequency-domain features were computed from the EMG data of 14 lower extremity muscles, while five time-domain features were calculated from GRF data during gait. Out of all the features computed for each subject, the principal component analysis (PCA) yielded 15 principal components that coupled both time and frequency domains (TFD). Further, the kNN model classified SS, MS and HC from each other by these 15 TFD features. The model was trained and validated using 32 and 21 EMG and GRF data datasets during gait, respectively. The classification and validation accuracy of 90.6% and 85.7% were obtained among SS, MS and HC. The proposed model is capable of early detection of AIS and can be used by medical professionals to plan treatments and corrective measures.

© 2022 Nalecz Institute of Biocybernetics and Biomedical Engineering of the Polish Academy of Sciences. Published by Elsevier B.V. All rights reserved.

* Corresponding author at: Centre for Biomedical Engineering, Indian Institute of Technology Delhi, New Delhi 110016, India.

E-mail address: dineshk@cbme.iitd.ac.in (D. Kalyanasundaram).

1. Introduction

Adolescence idiopathic scoliosis (AIS) is one of the most common spine deformities, affecting 1 to 3 % of children between 10 and 16 years [1]. Patients with AIS have difficulty in both mobility and balance during dynamic activities, including walking, running, etc. [2]. If not corrected, AIS affects the organs and muscles significantly [1,2], leading to permanent disability. AIS, a three-dimensional deformity of the spine, affects the mediolateral and anterior-posterior torso coordination, resulting in abnormal gait patterns [3]. Epidemiological studies suggest that about 65% of scoliotic subjects are idiopathic [3]. Though the cause of AIS is still unknown, understanding it is crucial for prognosis and treatment. Scoliosis at early stages cannot be detected by the naked eye, and hence it is challenging to identify potential subjects. When detected at later stages, scoliosis demands multiple surgeries [4] and numerous exposures to radiation like X-rays, causing significant mental and physical trauma as well as a financial burden to the patient and the caretakers.

The two types of AIS are C-type and S-type; the severity of AIS is defined by calculating Cobb's angle using X-ray, CT-scan, MRI, other radiological imaging techniques and scoliometer [5–8]. In the S-type AIS, a double curve in both lateral aspects of the spine is noted, whereas, in the C-type, the curve is formed in one direction of the lateral aspect of the spine [9]. Out of the two types, S-type AIS cases' incidence is more prominent than C-type AIS [10]. Cobb's angle is interpreted by drawing a line along the edges of the top and bottom vertebrae of the scoliotic curve. Studies suggest that for subjects with Cobb's angle greater than 25° and less than 40°, orthoses are commonly prescribed [11]. Surgical corrections are considered for subjects with Cobb's angle higher than 50°. However, exceptions can be made where subjects with 35° Cobb's angle were considered for surgery [12].

The method of treatment depends on the type of deformity [13], the location of the curve [10,14,15] and the severity based on Cobb's angle [9,16,17]. Studies also suggest that because of the spinal deformity, the centre of pressure of the body shifts [18,19]. The treatments for the prevention and progression of AIS include exercise, application of orthosis and surgery. Although AIS affects the spine severely, other parts of the body are also affected because of the curve propagation [20]. Studies suggest that AIS is often responsible for nervous system disorders in the peripheral and central nervous systems [21]. Moreover, AIS in the thoracic region affects the ribs of the subject because of deformation in the superior and lateral costotransverse ligaments [22]. Another common underlying effect is the abnormal metabolic pathway [5]. Studies suggest that the improper alignment of the lumbar or thoracic region results in improper mass distribution. Hence, there are cases of size reduction in vital organs like the liver, pancreas etc., [21].

Locomotion is a vital part of day-to-day activities. Different locomotion patterns depend on the muscle forces and activations, joint kinematics, centre of gravity and spatial coordination [23]. AIS, a deformity in the spine, alters the centre of mass (COM) during gait, leading to irregular gait patterns and ground reaction forces [24]. Studies suggest considerable

differences between the gait of healthy control (HC) and AIS subjects, including decreased step length, decreased cadence, range of motion, and higher energy expenditure [23]. Previous studies have implicated that ground reaction force is crucial in understanding the abnormalities in gait patterns [23,25].

Moreover, an electromyogram (EMG) has been used to detect muscle activations during gait and other physiological movements [17,26]. Literature suggests that the effect of muscle activations and ground reaction forces (GRF) are cardinal in extracting the features required to quantify the effect of AIS on gait. Table 1 contains a few works of literature on the effect of AIS on Electromyography (EMG) patterns, Spatio-temporal data, kinematics of walking, and ground reaction force (GRF). A few literatures were compared in the supplementary Table S1. There are studies involving mathematical models and gait on scoliosis. However, the effect of AIS on muscle activation and GRF of the lower extremity muscles is a gap in the literature.

In earlier studies by the authors of this manuscript, a statistical comparison of the gait pattern of congenital and AIS was carried out [27]. It was observed that most of the severe AIS subjects are from low and medium-income families in India, hence restricting them socially and economically for treatments. The subjects seek medical treatment only at a severe stage, where surgical correction is cardinal. Moreover, most mild scoliotic subjects are unaware of their present condition and chances of non-surgical recovery if treated early. Studies suggest that after Cobb's angle of 30° to 35°, the curve is prominent, and the subject experiences pain or other discomforts [3].

Hatzilazaridis et al. analysed the responses of postural muscles to galvanic vestibular stimulation for AIS and observed that the smaller ankle muscle response as well as delayed postural shift was prominent in AIS subjects [16]. Zhu et al. analysed the foot posture and walking performance of mild, moderate and severe AIS subjects. The authors observed significant difference in the gait of severe vs. moderate AIS, however, statistical differences between mild and healthy controls could not be observed [23]. This prompts for distinguishing AIS at early stages. Yoo et al. studied the significance of curve progression in children with scoliosis, lumbar lordosis, pelvic obliquity, and vertebral rotation. Severe impaired gross motor function, pelvic obliquity, vertebral rotation and female sex was found significantly related to curve progression [12]. Henceforth, this study aims to develop a methodology to detect AIS even at milder stages using EMG and GRF data. This will help in detecting AIS at the mild stages.

The EMG data showed similar activation for the muscles between MS and HC. Also, the ground reaction forces are similar for MS and HC. In short, it was challenging to identify MS AIS subjects either by the naked eye or via raw data of EMG or GRF. Hence, in this work, we have developed a supervised learning model based on EMG and GRF data to classify SS and MS from HC. Twenty-seven features from EMG data of fourteen lower extremity muscles were extracted, and five features from GRF data per subject. Further, the feature reduction technique was used to determine the distinguishable features extracted from the static pose and dynamic

Table 1 – Literature for effect of AIS on gait.

Author Group	Patient Diagnosis	Gender/type of patient	Type of Data	Configuration of data	Number of muscles involved in the study	Reference
Ram Haddas et al. 2019	Adult degenerative scoliosis (ADS)	20 (13 female and 7 male) ADS patients with symptomatic degenerative with three controls: 1) with walking sticks; 2) with walker; and 3) without any external device. Age: 63.00 ± 13.20 years	EMG	16-channel Delsys Trigno unit. Protocol not mentioned	8 muscles; External Oblique, Erector Spinae, Multifidus, Gluteus maximus, rectus femoris, Semitendinosus, Tibialis Anterior, Medial gastrocnemius	[17]
Holewijn et al. (2017)	AIS	18 AIS; Female, between 12 and 18 years	Spatio-temporal kinematic	VICON	No muscles	[42]
Holewijn et al. (2016)	AIS	12 AIS; Female patients	Spatio-temporal, kinematic	VICON; Measured at different speeds in treadmill for pre and post op cases	No muscle	[48]
Ioannis Hatzilazaridis et al. (2019)	AIS	12 Female adolescence age: 14.24 ± 1.61 yrs	Spatio-temporal data and EMG	Bonita 3, Nexus Vicon	8 muscles	[16]
Wu et al. (2019)	AIS	16 Female AIS and 16 healthy control	Kinematics and GRF	Vicon MX T-40, OMG, UK OR6-7, AMTI, USA force plates	No muscle activations were recorded	[33]
Haddas et al. (2018)	Adult Degenerative Scoliosis (ADS)	20 ADS	EMG	Delsys system (2,000 Hz)	8 muscles	[11]
Jafarnezhadgero et al. (2019)	HC	29 HC (12 females, 17 males)	GRF and EMG	Bertec Corporation, Columbus, OH, USA force plate	8 muscles	[34]
Syczewska et al. (2020)		30 cerebral palsy, 24 scoliosis, 30 S subjects	Spatio temporal data	VICON 460 system	No muscle activations were recorded	[49]
Pesenti et al. (2020)	AIS	22 females	Kinematics And imaging	In house	No muscle activations were recorded	[2]

walking data. A novel feature was computed from the GRF data correlated to the centre of pressure (COP) for the subjects and, in turn, defines equilibrioception. A k-nearest neighbour (kNN) model is proposed in this work to distinguish between severe AIS, mild AIS and HC. The developed model was trained with 32 datasets and validated with 21 EMG and GRF datasets during gait for SS, MS and HC.

2. Methods

2.1. Study preparation and data acquisition

The criteria for inclusion of the subjects were the following: (a) Age Range – 12–22 years, (b) Gender – Female, (c) Cobb's angle (HC < 20°, 20° < MS < 40°, SS > 40°) (d) Range of height – 130–170 cm and (e) Range of weight – 25–65 kg. The AIS subjects with other neurodegenerative disorders like ataxia, dystonia, Parkinson's, etc., were excluded from the study. [Table S2 in the supplementary](#) is provided for the inclusion and exclusion criteria used in this study. All the subjects belonged to Indian ethnicity predominantly from families with low and medium income (less than USD 70 a month).

This study analyses EMG and GRF data captured from (a) nine severe (SS) (Cobb's Angle > 40°), (b) three mild (MS) (20° < Cobb's Angle < 40°) AIS female patients (Curve type - S) and (c) four healthy (HC) female subjects. The AIS subjects' EMG and GRF data were captured before surgery, and the ages of the subjects ranged between 12 and 22 years. From all the above subjects, one dataset was captured in static pose (standing), and about 2–6 trials were captured during gait (walking) per subject, depending on the subject's comfort level. [Table 2](#) shows the nomenclature of the subjects and datasets of gait used for training and subsequent validation. Each of the subjects freely volunteered and signed the consent form for participation in the study. The study was approved by the ethics committee of All Indian Institute of Medical Science (AIIMS), New Delhi with reference number IEC/671/07.12.2018. The kinematic data, EMG and GRF, were recorded in the gait lab using SMART DX100 (BTS Bioengineering, Quincy, USA). Helen Hayes protocol was used to place the markers at the anatomical positions at a sampling rate of 500 Hz. The anthropometric data are provided in the [supplementary Table S3](#) for reference. The GRF data were extracted at a sampling rate of 1000 Hz. The synchronization unit of SMART DX100 up samples the EMG data to 1000 Hz. The kinematic marker positions and raw EMG and GRF from SMART DX 100 were saved as a c3d file. Mokka® (Version 0.6.2, 64 bit, Windows, Biomechanical ToolKit), open-source software, was employed to extract and convert the raw EMG and GRF data into ASCII files for further processing. The ASCII file was then exported into excel for database management. A fourth-order high pass Butterworth filter was used to filter the noise from the raw EMG data at a critical frequency of 6 Hz [28]. [Fig. 1](#) shows an AIS subject walking on the force plate in the gait lab. The flow chart for the study is shown in [Fig. 1 \(c\)](#).

2.2. Feature extraction

2.2.1. Pre-processing of EMG

All the data were centralized (cEMG) (Eq. [\(1a\)](#)), normalized (nEMG) (Eq. [\(1b\)](#)) between -1 and 1, followed by filtration before the computation of the features.

$$cEMG_i = EMG_i - \text{mean}(EMG) \quad \forall i = 1 \text{ to } N \quad (1a)$$

$$nEMG_i = 2 \frac{cEMG_i - \text{min}(cEMG_i)}{\text{max}(cEMG_i) - \text{min}(cEMG_i)} - 1 \quad \forall i = 1 \text{ to } N \quad (1b)$$

where N is the size of each EMG matrix.

2.2.2. Statistical analysis

The reliability of the data was evaluated using the test-retest methodology [29]. The normalized EMG for each subject was used to formulate the analysis. The coefficient of multiple correlations (CMC) was used to quantify the reliability of the between-day trials. Eq. [\(2\)](#) was used to calculate the CMC.

$$CMC = \sqrt{\frac{\sum_{i=1}^p \sum_{j=1}^q \frac{(nEMG_{ij} - \bar{nEMG}_j)(nEMG_{ij} - \bar{nEMG}_i)}{m(n-1)}}{\sum_{i=1}^p \sum_{j=1}^q \frac{(nEMG_{ij} - \bar{nEMG})^2}{(mn-1)}}} \quad (2)$$

where $nEMG_{ij}$ is the normalized EMG value for the i^{th} subject and j^{th} trial. \bar{nEMG}_j is the mean EMG signal during the trial j . \bar{nEMG} is the total mean EMG for all subjects and trials. p is the total number of trials in a group and q is the number of trials per subject within each group. From all the subjects, one trial was captured in static pose (standing) and about 2 to 6 trials were captured during gait (walking) per subject depending on the comfort level of the subject. Between any two walking trials that were essentially at different time periods T_i and T_j , CMC values were calculated.

2.2.3. EMG features

Eighteen time-domain features and nine frequency-domain features were extracted from EMG data of 14 lower limb muscles including the right 'R' and left 'L' extremities, namely, the erector spinae iliocostalis (Resi, Lesi), gluteus medius (Rgm, Lgm), biceps femoris caput longus (Rbfcl, Lbfcl), semimembranosus (Rs, Ls), gastrocnemius lateralis (Rgl, Lgl), rectus femoris (Rrs, Lrs) and tibialis anterior (Rta, Lta). Two strides per trial were used for extracting the features. The raw EMG data collected from the 14 lower extremity muscles are shown in [Supplementary Fig. S1](#). The mathematical equations used to calculate the EMG features are as follows:

2.2.3.1. Time domain EMG features. Eighteen-time domain features were calculated from the filtered EMG. The names and the equations for the calculation of each feature are given in Eq. [\(3a\)](#) to [\(4i\)](#).

Integrated EMG [30],

$$iav = \sum_{i=1}^N |nEMG_i| \quad (3a)$$

where, N represents the size of nEMG.

Mean Absolute Value [31],

Table 2 – Sample and trial description for training and validation data.

Type	Subject No.	No. of datasets for walking	Datasets used for Training	Datasets used for Validation
Severe Scoliotic (SS)	SS1	W1, W2	SS1_W1, SS1_W2	–
	SS2	W3, W4, W5	SS2_W3, SS2_W5	SS2_W4
	SS3	W6, W7, W8, W9	SS3_W6, SS3_W7	SS3_W9
	SS4	W10, W11, W12, W13	SS4_W11, SS4_W12	SS4_W13
	SS5	W14, W15, W16	SS5_W15, SS5_W16	–
	SS6	W17, W18, W19, W20	SS6_W18, SS6_W19	SS6_W17, SS6_W20
	SS7	W21, W22, W23, W24	SS7_W21, SS7_W22	SS7_W24
	SS8	W25, W26, W27	SS8_W25, SS8_W27	SS8_W26
	SS9	W28, W29, W30, W31	SS9_W28, SS9_W29	SS9_W30
Mild Scoliotic (MS)	MS1	W32, W33, W34, W35	MS1_W33, MS1_W34	MS1_W32, MS1_W35
	MS2	W36, W37, W38, W39	MS2_W37, MS2_W38	MS2_W36, MS2_39
	MS3	W40, W41, W42, W43	MS3_W41, MS3_W43	MS3_W40, MS3_W42
Healthy Control (HC)	HC1	W44, W45, W46, W47, W48	HC1_W44, HC1_W46	HC1_W45
	HC2	W49, W50, W51, W52	HC2_W49, HC2_W51	HC2_W52
	HC3	W53, W54, W55, W56, W57	HC3_W53, HC3_W54	HC3_W55, HC3_W56, HC3_W57
	HC4	W58, W59, W60, W61, W62, W63	HC4_W59, HC2_W61	HC4_W58, HC4_W60
Total	16	63	32	21
W: Walking data				

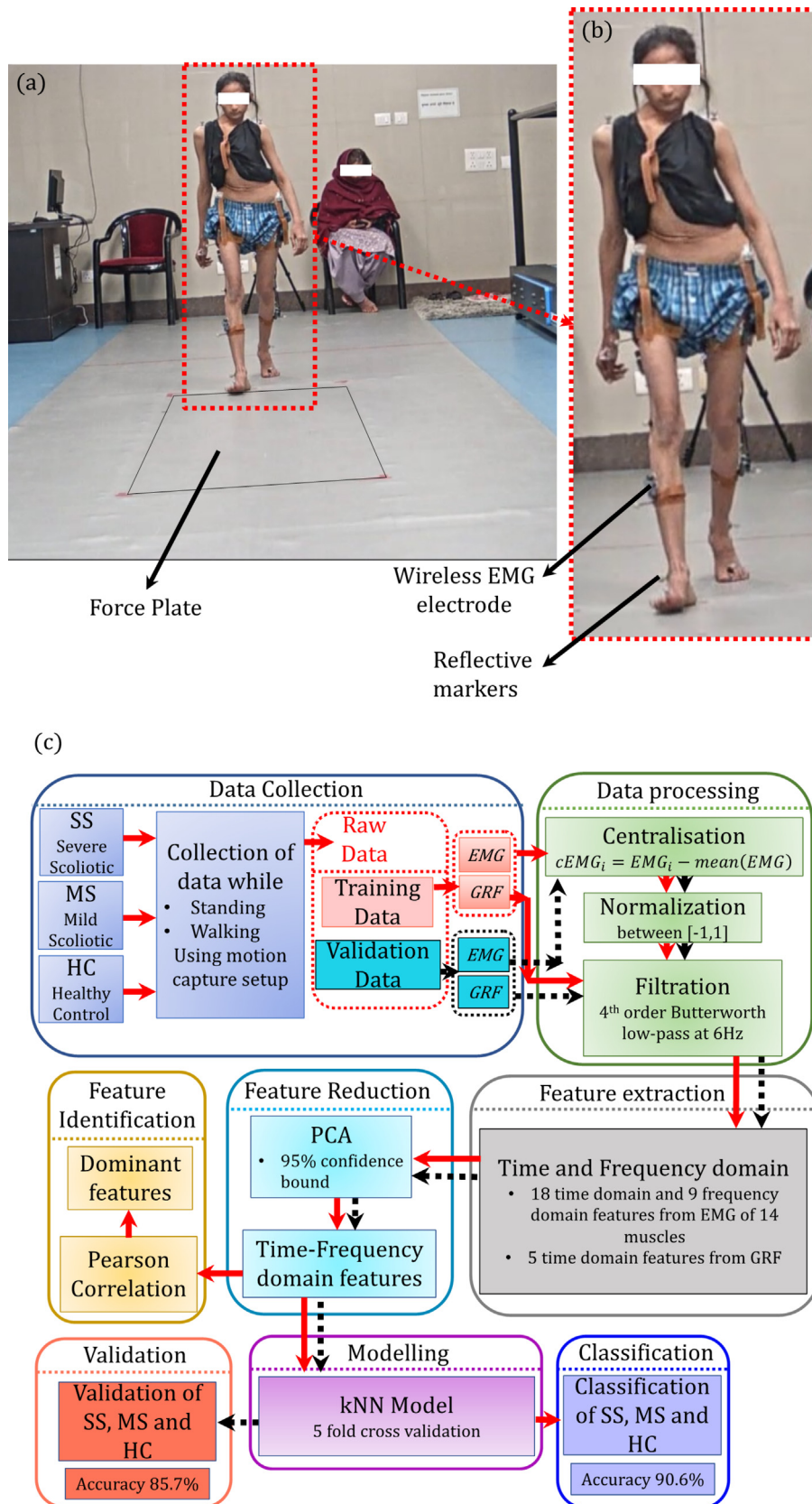


Fig. 1 – Representation of: (a) the gait lab; (b) AIS subject; (c) Flowchart of the work.

$$\text{mav} = \frac{1}{N} \sum_{i=1}^N |\text{nEMG}_i| \quad (3b)$$

Slope sign change [32],

$$\text{ssc} = \sum_{i=2}^{N-1} [h((\text{nEMG}_i - \text{nEMG}_{i-1}) \times (\text{nEMG}_i - \text{nEMG}_{i+1}))] \quad (3c)$$

$$\text{where, } h = \begin{cases} 1 & , \text{ if } \text{nEMG}_i \geq \text{threshold} \\ 0 & , \text{ otherwise } \end{cases}$$

Waveform Length [30],

$$\text{wl} = \sum_{i=1}^{N-1} |\text{nEMG}_{i+1} - \text{nEMG}_i| \quad (3d)$$

Zero crossing [32],

$$\text{zc} = \sum_{i=1}^{N-1} [\text{sg}(\text{nEMG}_i \times \text{nEMG}_{i+1}) \cap |\text{nEMG}_i - \text{nEMG}_{i+1}|] \quad (3e)$$

$$\text{where } \text{sg} = \begin{cases} 1 & , \text{ if } \text{nEMG}_i \geq \text{threshold} \\ 0 & , \text{ otherwise } \end{cases}$$

Average amplitude change [30],

$$\text{aac} = \frac{1}{N} \sum_{i=1}^{N-1} |\text{nEMG}_{i+1} - \text{nEMG}_i| \quad (3f)$$

Difference absolute standard deviation value [30],

$$\text{dasdv} = \sqrt{\frac{1}{N-1} \sum_{i=1}^{N-1} (\text{nEMG}_{i+1} - \text{nEMG}_i)^2} \quad (3g)$$

Log detector [30],

$$\text{ld} = e^{\frac{1}{N} \sum_{i=1}^N \log(|\text{nEMG}_i|)} \quad (3h)$$

Myopulse percentage rate [30],

$$\text{myop} = \frac{1}{N} \sum_{i=1}^N [\text{g}(\text{nEMG}_i)] \quad (3i)$$

$$\text{where } \text{g}(\text{x}_i) = \begin{cases} 1, & \text{if } \text{nEMG}_i \geq \text{threshold} \\ 0, & \text{otherwise} \end{cases}$$

Modified mean absolute value 1 [30],

$$\text{mmav} = \frac{1}{N} \sum_{i=1}^N \omega_i |\text{nEMG}_i| \quad (3j)$$

$$\text{where } \omega_i = \begin{cases} 1, & \text{if, } 0.25N \leq i \leq 0.75N \\ 0.5, & \text{otherwise} \end{cases}$$

Modified mean absolute value 2 [30],

$$\text{mmav2} = \frac{1}{N} \sum_{i=1}^N \omega_i |\text{nEMG}_i| \quad (3k)$$

$$\text{where } \omega_i = \begin{cases} 1, & \text{if, } 0.25N \leq i \leq 0.75N \\ \frac{4i}{N}, & \text{elseif, } i < 0.25N \\ \frac{4(i-1)}{N}, & \text{otherwise} \end{cases}$$

Simple square integral [30],

$$\text{ssi} = \sum_{i=1}^N \text{nEMG}_i^2 \quad (3l)$$

Variance of EMG [30],

$$\text{var} = \frac{1}{N-1} \sum_{i=1}^N \text{nEMG}_i^2 \quad (3m)$$

Willison amplitude [30],

$$\text{wamp} = \sum_{i=1}^{N-1} [k(|\text{nEMG}_i - \text{nEMG}_{i+1}|)] \quad (3n)$$

$$\text{where } k(x_i) = \begin{cases} 1, & \text{if } \text{nEMG}_i \geq \text{threshold} \\ 0, & \text{otherwise} \end{cases}$$

Maximum Fractal Length [30],

$$\text{mfl} = \log_{10} \left(\sqrt{\sum_{n=1}^{N-1} (W_{n+1} - W_n)^2} \right) \quad (3o)$$

where W_n is the wavelet coefficient with N as the total length of coefficient.

Absolute value of the 3rd, 4th, and 5th temporal moment [30],

$$\text{tm3} = \left| \frac{1}{N} \sum_{i=1}^N \text{nEMG}_i^3 \right| \quad (3p)$$

$$\text{tm4} = \left| \frac{1}{N} \sum_{i=1}^N \text{nEMG}_i^4 \right| \quad (3q)$$

$$\text{tm5} = \left| \frac{1}{N} \sum_{i=1}^N \text{nEMG}_i^5 \right| \quad (3r)$$

2.2.3.2. Frequency domain features. Mean Frequency [30],

$$\text{meanFreq} = \frac{\sum_{j=1}^M f_j W_j}{\sum_{j=1}^M W_j} \quad (4a)$$

where

f_j is the frequency of nEMG_i . W_j is the power spectral density of x_i , given by $W_j = |X_j|^2$, where X_j is the Fourier transform of nEMG_i .

Median Frequency [30],

$$\text{medFreq} = \sum_{j=1}^M W_j = \sum_{j=\text{medFreq}}^M W_j = 0.5 * \sum_{j=1}^M W_j \quad (4b)$$

Peak Frequency [30],

$$\text{peakFreq} = \max(W_j); j = 1, \dots, M \quad (4c)$$

Mean Power [30],

$$\text{meanPow} = \frac{\sum_{j=1}^M W_j}{M} \quad (4d)$$

Total Power [30],

$$\text{totPow} = \sum_{j=1}^M W_j = \text{sm0} \quad (4e)$$

The 1st, 2nd and 3rd spectral moments [30],

$$\text{sm1} = \sum_{j=1}^M W_j f_j \quad (4f)$$

$$\text{sm2} = \sum_{j=1}^M W_j f_j^2 \quad (4g)$$

$$\text{sm3} = \sum_{j=1}^M W_j f_j^3 \quad (4h)$$

Variance of central frequency [30],

$$vcf = \frac{1}{sm0} \sum_{j=1}^M W_j (f_j - f_c)^2 = \frac{sm2}{sm0} - \left(\frac{sm1}{sm0} \right)^2 \quad (4i)$$

2.2.4. GRF features

GRF data was extracted from the.c3d file using Mokka® and saved as a.csv file. Similar to the EMG data, the GRF data were pre-processed in MATLAB by centralising the data about the mean. Five features were calculated from the GRF data. COP value for standing and walking was calculated using force vector transpositions and vector additions. To understand the equilibrioception of the subject during walking, the anterior-posterior and medial-lateral sway of the body was calculated during both standing and walking. Moreover, the spatial orientation of the GRF vector was also calculated using three directional vectors, namely, alpha, beta, and gamma shift. The root-mean-square value of these parameters was calculated for feature extraction. The ground reaction vectors of both the limbs for AIS and HC are provided in the [supplementary Figure S2](#).

2.2.4.1. Center of pressure (COP). The force vector obtained from GRF data was decomposed into three orthogonal components (F_x , F_y and F_z) and their respective moments (M_x , M_y and M_z). At certain frames during gait, few of the subjects stepped between two adjacent force plates. Hence, two force vectors were prominent from two different force plates at these frames. Moreover, during the terminal stance to the pre-swing phase of gait, both the feet of the subject generate force vectors. Hence, each component of the force/moment vectors was bifurcated as two force/moment matrices, for instance, F_{xleft} and F_{xright} . Further, a force/moment vector was calculated for each bifurcated vector by taking the vector summation of forces at each frame given by Eqs. (5a) and (5b).

$$F_{x_L} = \begin{pmatrix} F_{xleft} & ; \text{ for standing - vector} \\ \sum_i^n F_{xlefti} & ; \text{for walking - matrix} \end{pmatrix} \quad (5a)$$

$$F_{x_R} = \begin{pmatrix} F_{xright} & ; \text{ for standing - vector} \\ \sum_i^n F_{xrighti} & ; \text{for walking - matrix} \end{pmatrix} \quad (5b)$$

where n is the number of force plates activated during the stride. Similarly, F_{y_L} , F_{y_R} , F_{z_L} , F_{z_R} , M_{x_L} , M_{x_R} , M_{y_L} , M_{y_R} , M_{z_L} and M_{z_R} were calculated for each limb. The coordinates of COP were calculated as per Eq. (6a) and (6b).

$$x_{cop1} = \frac{-M_{y_L}}{F_{z_L}} \text{ and } y_{cop1} = \frac{-M_{x_L}}{F_{z_L}} \quad (6a)$$

$$x_{cop2} = \frac{-M_{y_R}}{F_{z_R}} \text{ and } y_{cop2} = \frac{-M_{x_R}}{F_{z_R}} \quad (6b)$$

The resultant centralised COP was calculated using Eq. (7a) and (7b)

$$x_{cop} = \frac{F_{z_L}}{F_{z_L} + F_{z_R}} (x_{cop1} + x_{cop2}) \quad (7a)$$

$$y_{cop} = \frac{F_{z_L}}{F_{z_L} + F_{z_R}} (y_{cop1} + y_{cop2}) \quad (7b)$$

The vector x_{cop} and y_{cop} represents the medial-lateral sway and the anterior-posterior sway of the subject, respectively. The root-mean-square value of these two parameters was extracted as *apRMS* and *mlRMS* features.

2.2.4.2. Alpha, beta and gamma shift. Alpha (α), beta (β) and gamma shift (γ) are defined as the angle subtended by the GRF vector with the directional axes of the force plate. It can be calculated using my Eq. (8).

$$\alpha = \tan^{-1} \left(\frac{F_x}{|F|} \right); \beta = \tan^{-1} \left(\frac{F_y}{|F|} \right); \gamma = \tan^{-1} \left(\frac{F_z}{|F|} \right) \quad (8)$$

where $F_x = F_{x_L} - F_{x_R}$; $F_y = F_{y_L} - F_{y_R}$; $F_z = F_{z_L} + F_{z_R}$ and $|F| = \sqrt{(F_x^2 + F_y^2 + F_z^2)}$.

2.2.4.3. Centralization of the data. Feature matrices (14 muscles \times 27 EMG features + 5 GRF features = 383 features) corresponding to SS, MS and HC were centralized using the Equations (9a), (9b) and (9c) as per the number of gait trials.

$$\widehat{FM}_{SS} = FM_{SS} - \bar{FM}_{SS} \quad (9a)$$

where $\bar{FM}_{SS} = \frac{\sum_{i=1}^{36} \sum_{j=1}^{383} FM_{ij}}{36 \times 383}$

$$\widehat{FM}_{MS} = FM_{MS} - \bar{FM}_{MS} \quad (9b)$$

where $\bar{FM}_{MS} = \frac{\sum_{i=1}^{12} \sum_{j=1}^{383} FM_{ij}}{12 \times 383}$

$$\widehat{FM}_{HC} = FM_{HC} - \bar{FM}_{HC} \quad (9c)$$

where $\bar{FM}_{HC} = \frac{\sum_{i=1}^{16} \sum_{j=1}^{383} FM_{ij}}{16 \times 383}$

The concatenation of the three matrices yields the total feature matrix \widehat{FM} of size 64×383 .

2.3. Feature reduction

A covariance matrix was calculated from the feature matrix (383 features by 64 strides). The diagonal elements of the covariance matrix were extracted. These diagonal elements of the covariance matrix (COV) were ranked in ascending order of value. Single value decomposition was used on the ascending COV to calculate the principal components representing time-frequency domain features. Here, F represent the features set matrix of order m by n , where m corresponds to the sample size and n indicates the number of features extracted. The following steps were adopted to calculate the principal components.

The covariance matrix COV is calculated using Eq. (10).

$$COV = \frac{1}{m} [\widehat{FM} \cdot \widehat{FM}^T] \quad (10)$$

where m is 64. Using the Cayley Hamilton theorem, the eigenvalues and the eigenvectors were calculated from Eq. (11).

$$(COV - \lambda)I = 0 \quad (11)$$

where I is an identity matrix of size m by m , and λ indicates the eigenvalues. The eigenvalues are arranged in descending order. The eigenvector corresponding to the highest eigenvalue is the first principal component, and so on. The code

was executed in MATLAB. Sixty-four time-frequency domain features (TFD) combined with 383 features were calculated using PCA. These TFD features were subjected to a 95% confidence bound on their eigenvalues to evaluate fifteen principal component features, namely PC1-PC15. These fifteen principal features were used to create the classification model.

2.4. Classification and validation

SS subjects can be differentiated visually from HC. However, this is not the case with MS subjects, as there are minute gait changes from HC. Initially, features from the subjects' standing data were collected and used for classifying SS, MS and HC. However, the classification accuracy was low, i.e. ~65%. The algorithm used for classification using standing data was a support vector machine (SVM). The confusion matrix and details about SVM are provided in the supplementary section with [Fig. S3](#). Therefore, to differentiate AIS from HC at an early stage, the walking data of the subjects were recorded. After feature extraction, k-nearest neighbour (kNN) with five folds of cross-validation was used to classify SS, MS and HC. In kNN, the Euclidean distance of the new data point is calculated from other data points depending on the k value ([Fig. 4\(c\)](#)). For instance, if k = 5, the Euclidean distance of 5 data points are calculated in the vicinity of the new data point. The weighted count of the nearest neighbour is calculated. Based on the count, the decision is made to classify the new data point. The equation for calculating the Euclidean distance is given in [Eq. \(12\)](#).

$$D_i = \sqrt{\sum_{i=1}^N (x_{1i} - x_{2i})^2} \quad (12)$$

where D_i is the distance between the points x_1 and x_2 . N is the number of observations.

To use the model, the users can store the EMG data of 14 muscles and GRF data collected from one or multiple strides of walking of a subject in a.xlsx file or.csv file (MS Excel compatible). The complete model takes the.csv file as an input and classifies the subject as SS, MS or HC.

3. Results

The test-retest method was used to evaluate the reliability of the EMG and GRF data collected. The calculated values of CMC corresponding to the data for HC, MS and SS groups are given in the [supplementary Table S4](#). The correlation was found to be poor within groups for the trials. The weaker correlation is because of the variability in the kinematics during the subjects' gait. As the classification is not possible using CMC between the groups, a supervised learning-based algorithm was used in this work. Moreover, a comparison with previous literature for healthy control is provided in the [supplementary Fig. S4](#).

Principal components of 383 features constituting time-domain, frequency-domain components of EMG of 14 lower extremity muscles and GRF were evaluated. [Fig. 2](#) and [Fig. 3](#) show the parallel coordinate plots in terms of standard deviations of time-domain and frequency-domain features extracted from EMG and GRF data during one stride of the gait

cycle. However, due to space constraints, the parallel coordinate plots of some of the time domain features are presented in the [supplementary section \(Figure S5\)](#). It was observed that the frequency domain features illustrated lower covariance in the covariance matrix, which is evident from [Table 3](#), and hence were not considered. The principal components of the features were evaluated using single value decomposition. Out of the 64 principal components, fifteen were selected based on a 95 % confidence bound. [Fig. 4\(a\)](#) illustrates a scree plot of the Eigenvalues represented by the 64 principal components. [Fig. 4\(b\)](#) demonstrates the parallel coordinate plot of these fifteen principal components. These components combine one or more of the 383 feature sets and are represented as time-frequency domain features. The kNN model was used to classify the data into three classes, namely, severe scoliotic (SS), mild scoliotic (MS) and healthy control (HC). The accuracy of classification among SS, MS and HC was 90.6%. [Table 3](#) depicts the significant (greater than 0.9 and lesser than -0.9) Pearson Correlation Coefficient between features and the fifteen principal components. The Pearson Correlation Coefficient greater than 0.9 and lesser than -0.9 is considered significant in explaining linear correlation. Furthermore, 21 random trials were conducted to collect data for validation corresponding to eight SS, six MS and seven HC subjects. The accuracy of validation is 85.7%. [Fig. 5](#) depicts the confusion matrix for the training and validation data. [Fig. 6\(a\), \(b\) and \(c\)](#) shows the receiver operating characteristics (ROC) plot with SS, MS and HC as positive classes, respectively.

4. Discussion

The study's objective was to identify the activation of the muscles of AIS patients during gait. A KNN model has been proposed to classify the subjects based on their muscle activations and ground reaction forces during gait. In this study, the type of scoliosis curve for all the AIS subjects was of a similar curve (i.e. S-type curves). The curve was prominent in the lower thoracic region extending up to the lumbar region. SS subjects had slower speeds than MS and HC by ~12%. This was in accordance with the literature [\[33\]](#). Moreover, approximately 200 % variation in the GRF was exerted between the two lower extremities for SS subjects. This shows the improper mass distribution in the two halves of the SS subjects. The data for GRF during stance is shown in the [supplementary section \(Fig. S6\)](#).

In [Fig. 2](#) and [Fig. 3](#), it was observed that the muscles Resi, Lesi, Rgl, Lgl, Rgm and Lgm produced distinctive linear variations for different feature sets between HC and SS subjects. The time-domain features (iav, mav, ssc, zc, ld, myop, mmav, mmav2, ssl, var, tm3, tm4 and tm5) showed a clear distinction in terms of standard deviations between SS and HC. These muscles are highly affected due to AIS in SS subjects. Erector spinae iliocostalis (Resi and Lesi) originates from the sacrum, erector spinae aponeurosis and iliac crest and is responsible for the flexion of the pelvis. This muscle is also connected to the thoracic and lumbar region of the spine, and hence the activation of this muscle is highly affected by AIS. Compared to HC, this muscle in SS subjects shows

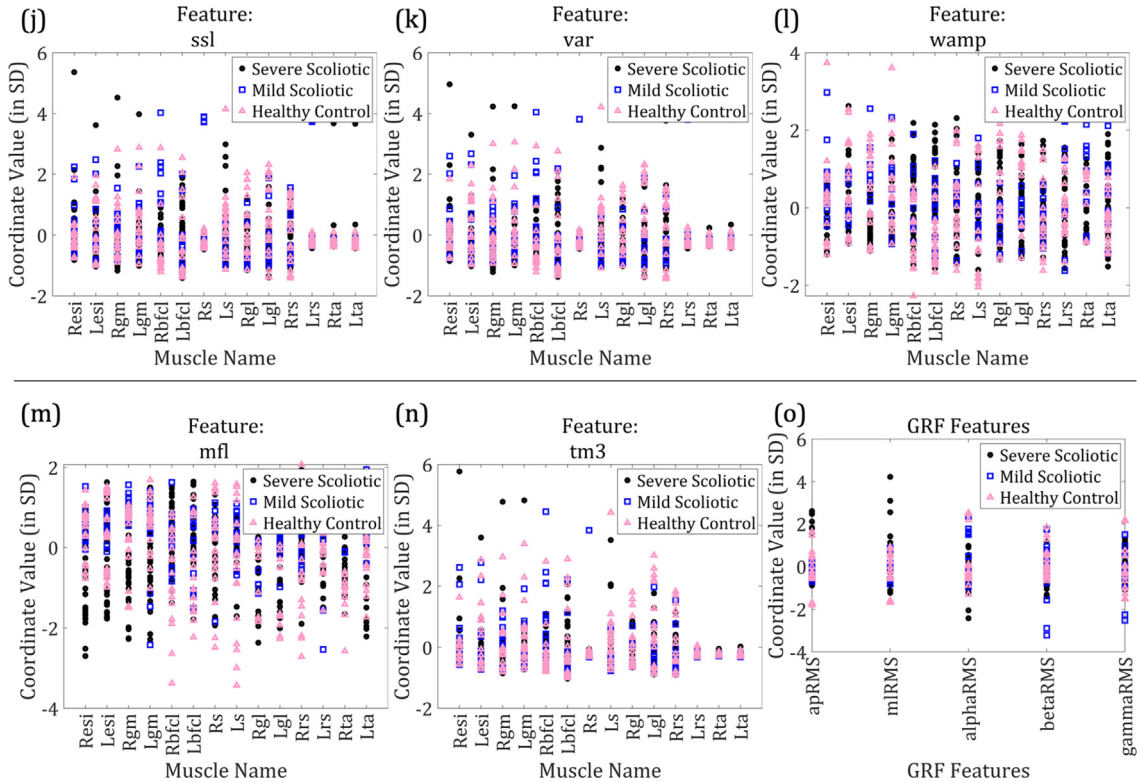


Fig. 2 – Time Domain features of EMG and GRF.

delayed activation during pelvic movement in gait [34]. Gluteus medius (*Rgm*, *Lgm*) are the pelvic joint's prime abductor muscle and are anatomically attached to the pelvis and medial part of the femur [34]. Its prime function is to stabilise the pelvis in a unilateral stance. It was observed that the activation of gluteus medius was delayed in AIS subjects compared to healthy subjects. This is because of the biomechanics of the pelvis during gait. During flexion of the pelvis joint in gait, a substantial amount of abduction occurs at the joint to balance the weight distribution of the subject. Gastrocnemius lateralis is anatomically attached to the lateral condyle of the femur, and its other end is connected to the calcaneus tendon. Due to delayed activation of erector spinae iliocostalis, the flexion of the knee is also affected, resulting in delayed activation of gastrocnemius lateralis [16]. This muscle is the prime muscle for flexion of the knee joint, and hence, a delayed response was observed in this muscle. There was a significant variation in the mean frequency power of SS and HC. This is because of the muscles' delayed response in SS subjects compared to HC.

It was observed that the matrix's dimensionality comprising the time and frequency domain features was large. Hence, PCA was used to reduce the dimensionality of the feature matrix, which resulted in 64 time-frequency domain features. Fig. 4(b) shows the parallel coordinate plot for all the fifteen PCA features. It is prominent from the features that PC1 shows distinct linear variation between SS and HC. However, the standard deviations of MS and HC tend to overlap. In PC2-PC15, the standard deviations of all the three classes overlap. The Pearson coefficient between the contributing features and the principal components is shown in Table 3. It was

observed that the principal component PC1 is dependent on the features iav, mav, ld, mmav, mmav2, ssl, var, tm3, tm4 and tm5 of the muscles *Lrs*, *Rta* and *Lta*. This implicates the significance of these features in the formulation of PC1. Principal component PC2 showed a linear correlation between iav, mav, ld, mmav, ssl, var, tm3, tm4 and tm5 for *Lrs* muscle, as shown in Table 3. PC3 demonstrated a linear correlation for iav, mav, ld, mmav, mmav2, ssl, var, tm3, tm4 and tm5 for *Rs* muscle. All other PCAs, i.e. PC4-PC15, show a minimum linear correlation with the feature sets, as demonstrated in Table 3.

Though the clear distinction between SS subjects can be made from HC subjects or MS subjects just by visual inspection, the challenge is when classifying MS and HC for early detection of AIS. The features extracted from the EMG and GRF data directly cannot differentiate MS and HC, as evident from Figs. 2, 3 and 4. Moreover, neither features showed linear variation between MS and HC, as evident from Table 3. Hence, supervised learning using the k-nearest neighbour method was used to classify all the three classes, i.e. SS, MS and HC. The kNN model was able to classify the three classes with overall training and validation accuracy of 90.6% and 85.7%, respectively.

Fig. 5 demonstrates the confusion matrix of the training data used in formulating the kNN model. During training, the true positive rate and positive predictive value of SS were 97% and 92%, respectively. As in SS subjects, Cobb's angle was higher than 40°, and high classification accuracy was expected. For MS subjects, the true positive rate and positive predictive value during training were 75% and 100%, respectively, acceptable as the false discovery rate is none. For HC,

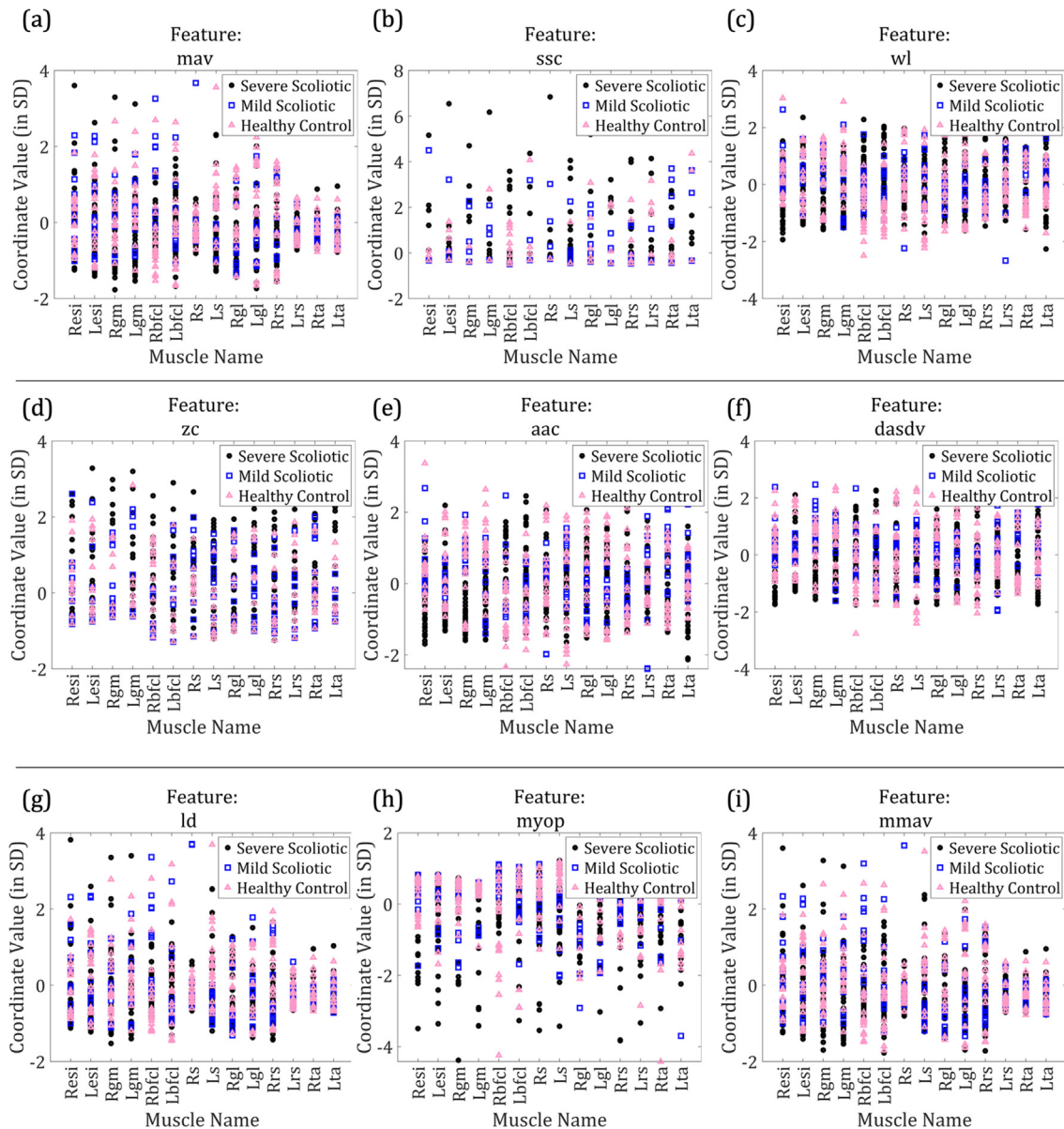


Fig 2. (continued)

the true positive rate and positive predictive values were 88% and 82%, respectively. The ROC plots (Fig. 6) for three classes, namely SS, MS, and HC as a positive class, show the relationship between the true positive rate and the false positive rate of the model. During validation, the model predicted 7 out of 8 trials for SS subjects, 5 out of 6 trials for MS subjects and 6 out of 7 trials for HC. Fig. 5(b) demonstrates the confusion matrix of the validation trials. The true positive rate and positive predictive value for SS subjects were 88% and 100%, respectively. For MS subjects, the true positive rate and the positive predictive value were 83% and 71%, respectively. Moreover, for HC, the positive predictive value and the true positive rate were 86%. Hence, the model can be used to detect of scoliosis at an early stage by using EMG data of 14 muscles and GRF data during one or multiple strides of a subject.

Corrective exercises and surgical interventions are the two modes of therapy for AIS. Zhou et al. studied the effect of

three-dimensional corrective exercise therapy (TDCE) on AIS subjects and control group [35]. The study concluded that TDCE, family rehabilitation and basic body therapy may help patients in adapting corrective exercises for AIS subjects. Moreover, research on biofeedback postural training on mild AIS subjects has the ability to reduce asymmetry in paraspinal muscle activities and hence control the scoliotic curve progression [36]. All non-operative measures demand a multidisciplinary approach for patient management [37], one that is resource and time-intensive. Park et al. studied the effect of schroth rehabilitation exercise program on feet and spine alignment in AIS subjects. It was found that schroth rehabilitation exercise had significant effect in improving the Cobb's angle, scoliometer readings, lumbar lordosis and calcaneal valgus angles [38]. Marin et al. used LiDAR and Kinect based imaging to execute the self-corrective movement strategy using Wilcoxon signed-rank test. Real-time changes were

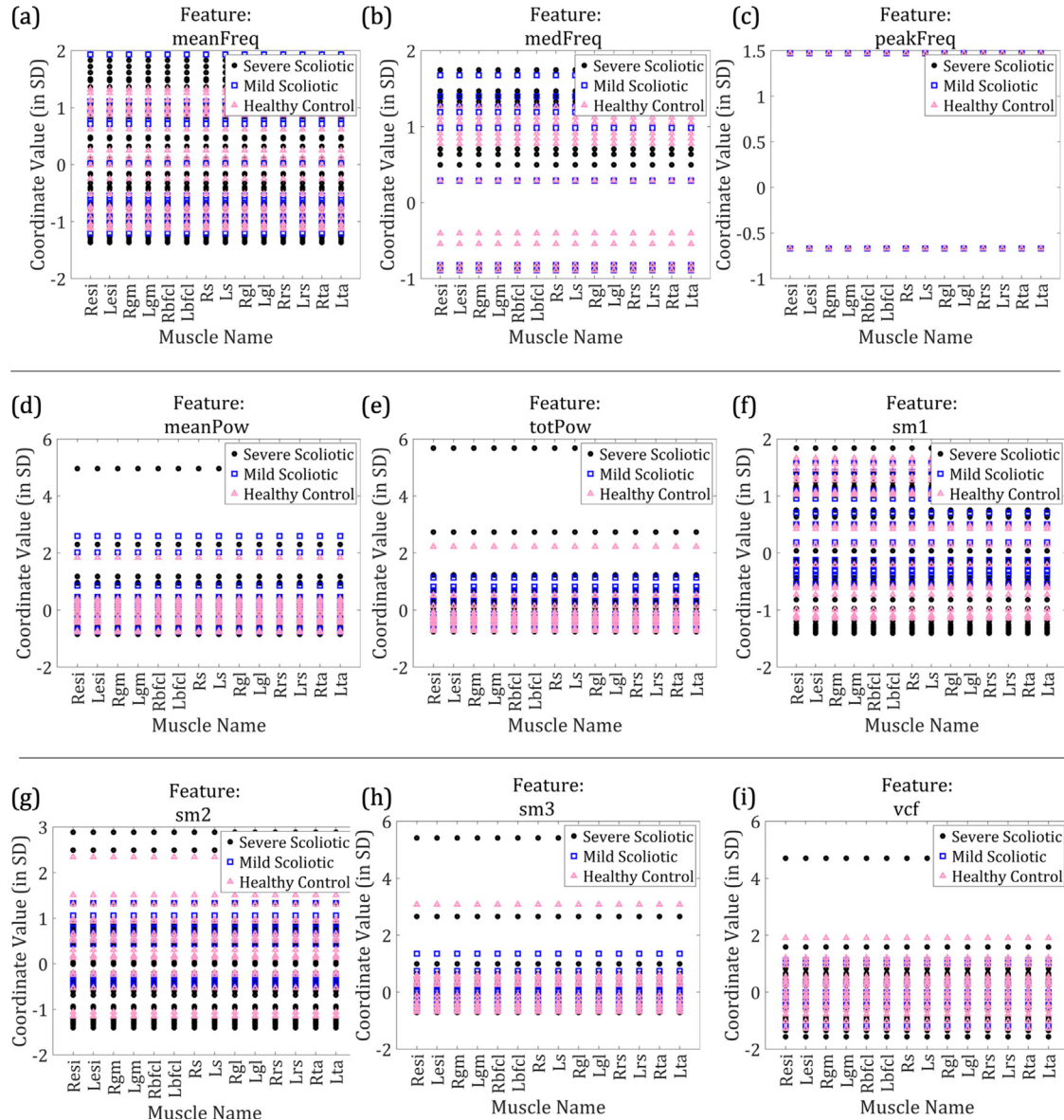


Fig. 3 – Frequency Domain features of EMG.

observed during the performance of self-corrective movement, affecting the curve correction [39]. Belli et al. evaluated the self-perceived body image and SRS-22 in mild AIS. There was significant statistical difference self-perceived body image and SRS-22 domain [7]. Samadi et al. identified the relevant intervertebral effort indicators during gait of AIS subjects. Statistical analysis using Kolmogorov-Smirnov and Two-sample t-test was performed on the data [40].

In the case of surgical intervention, significant improvement shall be observed on the scoliotic curve, however, the risk of such a surgical intervention is high [41]. Holewijn et al. studied the effect of spinal fusion on thoracic-pelvic range of motion during gait and found that there is a decrease in the range of motion post-surgery, especially at higher speeds of walking [42]. Pesenti et al. observed that significant symmetry was present in gait post-surgery. However, in the sagittal plane, thoracolumbar extension within the fused area

resulted in reduced extension of the cervicothoracic and lumbar region [43].

Several research groups have also attempted to classify AIS subjects. A brief comparison of the proposed model and other models reported in the literature is given in Table 4. Among the studies referred in Table 4, there are imaging-based deep neural network models to predict Cobb's angle from X-rays and CT data, with correlation coefficients varying from 0.77 to 0.95 [44,45]. These deep neural networks encompass complex algorithms over several layers (4 and above) compared to the current model based on an efficient supervised learning technique with two layers and within a similar range of accuracy. Kokabu et al. developed an deep learning based convolution neural network model from X-ray images [44] to predict the Cobbs's angle with an accuracy ranging from 81 to 95% which is greater than Wu et al.'s HRNet based classification model [45]. Many other studies (shown in

Table 3 – Pearson coefficients of prominent three features and corresponding muscles between features and principal components.

Feature Name	Muscle Name	Principal Components			Feature Name	Muscle Name	Principal Components		
		PC1	PC2	PC3			PC1	PC2	PC3
iav	Rs	-0.15	-0.36	0.91	ssl	Rs	-0.13	-0.35	0.92
	Lrs	-0.29	0.92	0.23		Lrs	-0.23	0.94	0.24
	Rta	0.95	0.12	0.08		Rta	0.98	0.1	0.1
	Lta	0.93	0.15	0.13		Lta	0.98	0.11	0.12
mav	Rs	-0.13	-0.36	0.91	var	Rs	-0.12	-0.35	0.92
	Lrs	-0.29	0.91	0.25		Lrs	-0.24	0.93	0.24
	Rta	0.95	0.11	0.1		Rta	0.98	0.1	0.1
	Lta	0.94	0.14	0.15		Lta	0.98	0.11	0.12
ld	Rs	-0.14	-0.36	0.91	tm3	Rs	-0.12	-0.34	0.92
	Lrs	-0.27	0.91	0.26		Lrs	-0.21	0.93	0.24
	Rta	0.95	0.11	0.08		Rta	0.98	0.1	0.1
	Lta	0.94	0.13	0.13		Lta	0.98	0.1	0.11
mmav	Rs	-0.13	-0.36	0.91	tm4	Rs	-0.12	-0.33	0.92
	Lrs	-0.29	0.9	0.25		Lrs	-0.2	0.93	0.24
	Rta	0.95	0.11	0.1		Rta	0.98	0.1	0.1
	Lta	0.94	0.14	0.15		Lta	0.98	0.1	0.11
mmav2	Rs	-0.12	-0.36	0.9	tm5	Rs	-0.12	-0.33	0.92
	Rta	0.95	0.12	0.11		Lrs	-0.2	0.93	0.24
	Lta	0.94	0.15	0.14		Rta	0.98	0.1	0.1
						Lta	0.98	0.1	0.1

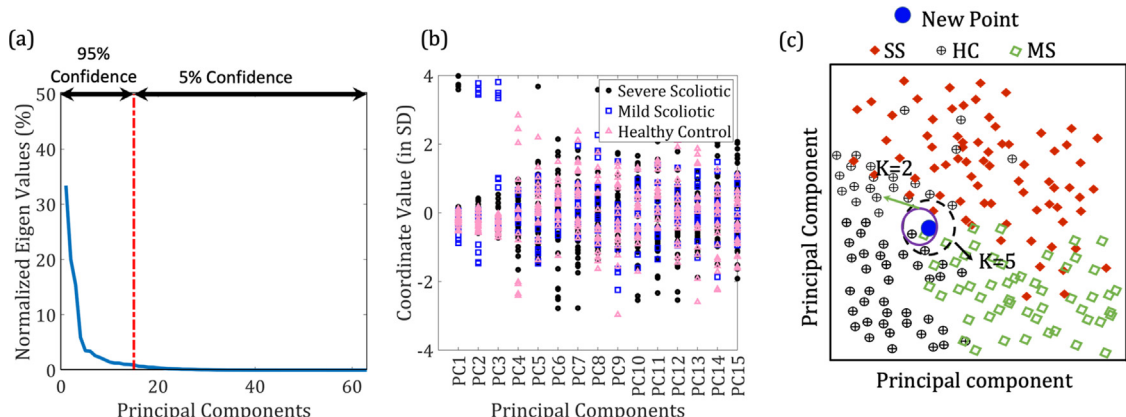


Fig. 4 – a) Scree plot at 95% confidence; (b) the principal components; (c) k-Nearest Neighbour classification of the new point (blue) between classes SS, MS and HC.

Table 4) have not reported the computational time and accuracy of the model. Caesarendra et al. developed an image based classification technique using deep learning based on convolutional neural network with an accuracy of 93.4% [46]. Tajdari et al. developed an 3D landmark based surface registration and neural network for spine shape prediction with an accuracy ranging from 94 to 99%. Peng et al. evaluated the effect of traditional Chinese health and fitness exercise towards the improvement of spinal health for scoliosis. The authors used multi view learning based on deep information from X-rays to evaluate the improvement [24]. Li et al. developed an automated scoliosis diagnostic platform based on deep learning (U-net segmentation) from X-rays with low error rate of 0.09–0.1 [47]. The proposed/developed

data-driven classification model classifies mild AIS from healthy controls using EMG and GRF data during walking at an accuracy of 86 %. This shall aid in the potential detection of mild AIS, thereby helping physicians to diagnose the condition and begin timely treatment.

Though the developed model has the ability to detect scoliosis at an earlier stage, however, there are certain limitations of this study. The collection of data is a time-intensive exercise and also demands a gait laboratory. Hence, the availability of such facilities in poor-resource economies is very limited. On the other hand, X-ray based imaging techniques are available (on a relative scale) easily and the analysis of images is quite straightforward; however, the collected data has the potential to bring greater clarity in classifying mild

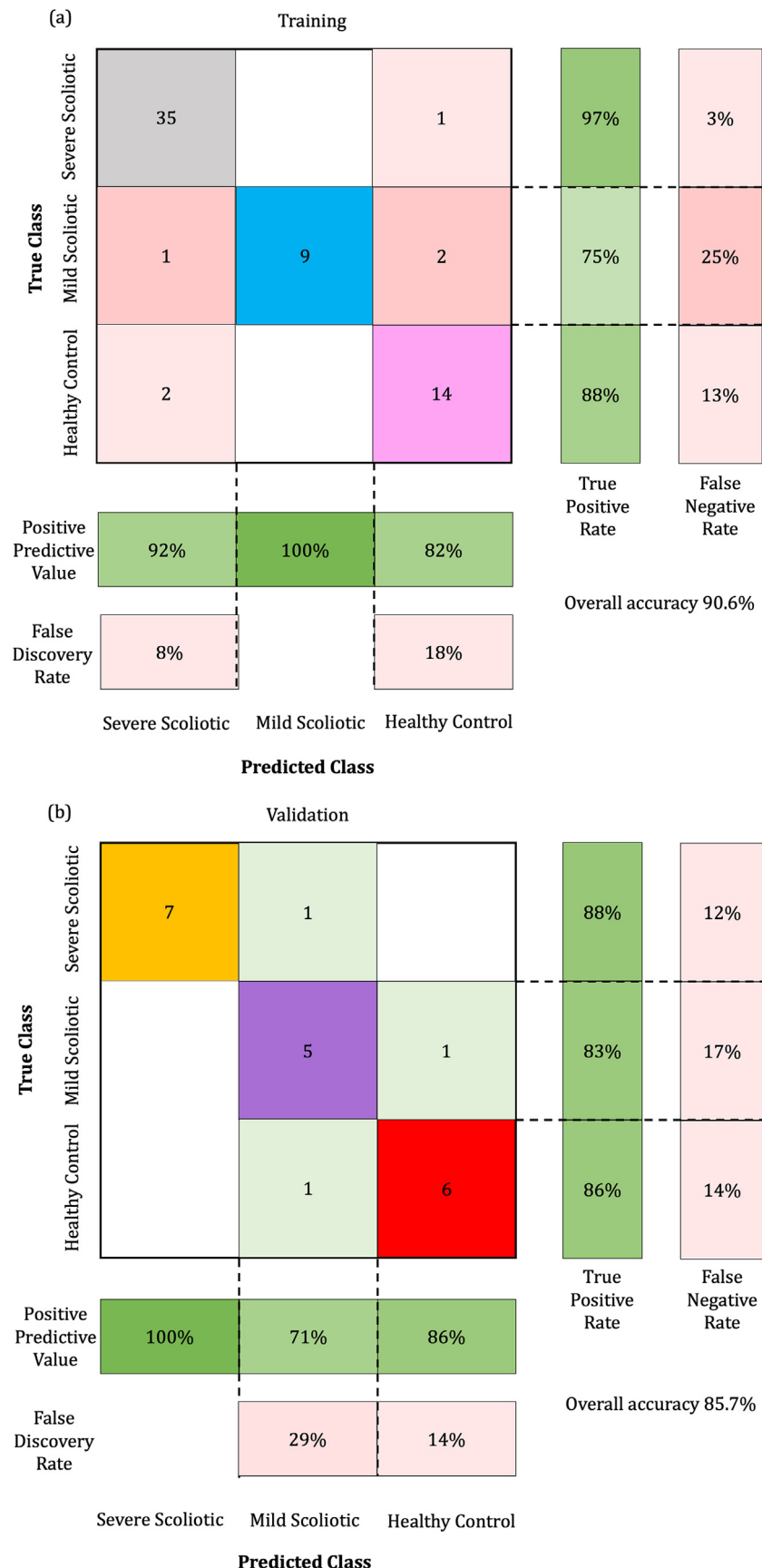


Fig. 5 – Confusion matrix of: (a) training data; (b) validation data.

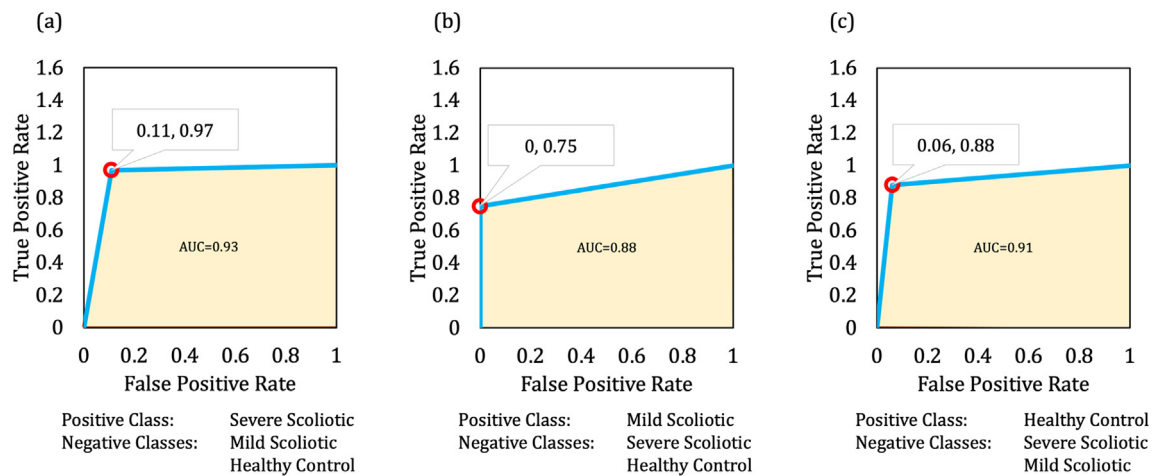


Fig. 6 – Receiver Operating Characteristic (ROC) of the model.

Table 4 – Comparison with similar studies with the proposed model for AIS.

Author Group	Patient Diagnosis	Type of analysis/Algorithm	Accuracy (% or error)	Reference
Holewijn et al. (2017)	AIS	Statistical	Not Reported	[42]
Hatzilazaridis et al. (2019)	AIS	Comparative	Not Reported	[16]
Zhu et al. (2021)	Healthy, Mild, Moderate and Severe AIS.	Statistical	Not Reported	[23]
Kokabu et al. (2021)	AIS	Deep learning with convolutional neural network from X ray Images	81–95%	[44]
Wu et al. (2022)	AIS	Deep learning (HRNet) from X ray Images	77.2–89.36%	[45]
Caesarendra et al. (2022)	AIS	Image-based classification using Deep learning based on CNN	93.4%	[46]
Yoo et al. (2022)	Scoliosis, Lumbar Lordosis, Pelvic Obliquity, Vertebral rotation	Linear mixed-effects model	Not Reported	[12]
Jiefu Peng (2022)	Scoliosis	Multiview Learning based on Deep Information from X rays	Not Reported	[24]
Tajdari et al. (2020)	AIS	3D landmark-based surface registration and neural network for spine shape prediction	94–99%	[8]
Park et al. (2022)	AIS, Lumbar lordosis, calcaneal valgus	Statistical	Not Reported	[38]
Li et al. (2022)	Scoliosis	Deep learning based on U-net segmentation from X rays	An error rate of 0.09–0.1	[47]
Marin et al. (2022)	AIS	Statistical analysis of LiDAR and Kinect based imaging	Not Reported	[39]
Belli et al. (2022)	AIS- Mild	Questionnaire and photogrammetry based statistical analysis	Not Reported	[7]
Pesenti et al (2021)	AIS	Statistical single centred prospective study	Not Reported	[43]
Samadi et al. (2020)	AIS	Statistical analysis of effort indicators in the spine using gait data	Not Reported	[40]
Proposed model	AIS	kNN based model	85.70%	NA

AIS from health controls. Currently, the proposed model cannot identify clinical features like muscle atrophy, severity scale, etc., which could be the future scope of work. Further, common problems with surface EMG placement, such as identification of the muscle belly, outliers caused by skin impedance, etc., are still a pitfall for the developed model. However, these outliers can be minimised using the SENIAM guidelines.

5. Conclusion

This study was focused on understanding the effect of severe (SS) (Cobb's angle $> 40^\circ$) and mild (MS) ($20^\circ < \text{Cobb's angle} < 40^\circ$) AIS on the muscle activation of 14 muscles in the lower extremity during walking. Moreover, the ground reaction force was also investigated and compared among SS, MS and healthy subjects (HC). It was observed that Erector spinae iliocostalis, Gluteus Medius, and Gastrocnemius lateralis are the primary muscles that affect the gait of SS subjects. A delayed response in these muscles was observed in SS compared to HC. The flexion and adduction of the hip joint proximal to the curve were readily affected because of SS. This resulted in an improper shift of the centre of mass during gait. A kNN model was trained and validated to classify and detect SS, MS and HC using EMG and GRF data during walking. The proposed model can be used to introspect AIS patients in their mild stages instead of exposing them to radiations like X-rays. Moreover, the EMG and GRF data of the SS subjects can be used to identify muscle atrophies for proper planning of surgical intervention. This can aid the researchers and medical practitioners in understanding and detect AIS in the mild phase, reducing the chances of surgical corrections and curve progression.

6. Ethical clearance

Ethical clearance for data collection was obtained from All Indian Institute of Medical Science (AIIMS), New Delhi with reference number IEC/671/07.12.2018 for AIS and HC.

7. Author's contribution

AS and DK formulated the study. MG and BG collected the data. AS and KV implemented the mathematical and statistical protocol for data analysis. AS and DK wrote the manuscript and edited it.

Declaration of Competing Interest

The authors declare that they have no known competing financial interests or personal relationships that could have appeared to influence the work reported in this paper.

Acknowledgements

We would like to acknowledge all the subjects who participated in the study and aided us with the data for AIS and Healthy Control.

Appendix A. Supplementary data

Supplementary data to this article can be found online at <https://doi.org/10.1016/j.bbe.2022.06.006>.

REFERENCES

- [1] Di Pauli T, von Treuheim DT, Li C, Mikhail D, Cataldo DR, Cooperman BG, et al. Reliable skeletal maturity assessment for an AIS patient cohort: external validation of the proximal humerus ossification system (PHOS) and relevant learning methodology. *Spine Deform* 2020;8:613–20. <https://doi.org/10.1007/s43390-020-00105-5>.
- [2] Pesenti S, Pomero V, Prost S, Severyns M, Authier G, Roscigni L, et al. Curve location influences spinal balance in coronal and sagittal planes but not transversal trunk motion in adolescents with idiopathic scoliosis: a prospective observational study. *Eur Spine J* 2020;29:1972–80. <https://doi.org/10.1007/s00586-020-06361-3>.
- [3] Haddas R, Kosztowski T, Mar D, Boah A, Lieberman IH. Balance effort, Cone of Economy, and dynamic compensatory mechanisms in common degenerative spinal pathologies. *Gait Posture* 2021;89:67–73. <https://doi.org/10.1016/j.gaitpost.2021.04.038>.
- [4] Sampiev MT, Zagorodniy NV, Lysenko IS, Dubinin IP, Chemurzieva KHM. Two-stage treatment of idiopathic scoliosis using the LSZ growing system with a 10-year follow-up: a case report. *J Surg Case Reports* 2022:1–3. <https://doi.org/10.1093/jscr/jac087>.
- [5] Machino M, Kawakami N, Ohara T, Saito T, Tauchi R. Factors affecting postoperative pulmonary function deterioration in adolescent idiopathic scoliosis: A prospective study using 3-dimensional image reconstruction by biplanar stereoradiography. *J Clin Neurosci* 2022;98:182–8. <https://doi.org/10.1016/j.jocn.2022.02.014>.
- [6] Zhu TB, Wang YS, Xie JM, Zhang Y, Zhao Z, Li T, et al. Development and initial validation of classification for severe spinal deformity based on X-ray features. *Eur Spine J* 2022;31:79–87. <https://doi.org/10.1007/s00586-021-07028-3>.
- [7] Belli G, Toselli S, Latessa PM, Mauro M. Evaluation of self-perceived body image in adolescents with mild idiopathic scoliosis. *Eur J Invest Heal Psychol Educ* 2022;12:319–33. <https://doi.org/10.3390/ejihpe12030023>.
- [8] Tajdari M, Pawar A, Li H, Tajdari F, Maqsood A, Cleary E, et al. Image-based modelling for Adolescent Idiopathic Scoliosis: Mechanistic machine learning analysis and prediction. *Comput Methods Appl Mech Eng* 2021;374:113590. <https://doi.org/10.1016/j.cma.2020.113590>.
- [9] Sung PS, Park MS. Compensatory ground reaction forces during scoliotic gait in subjects with and without right adolescent idiopathic scoliosis. *Symmetry (Basel)* 2021;13:2372. <https://doi.org/10.3390/sym13122372>.
- [10] Vergari C, Skalli W, Abelin-Genevois K, Bernard JC, Hu Z, Cheng JCY, et al. Effect of curve location on the severity index for adolescent idiopathic scoliosis: a longitudinal cohort study. *Eur Radiol* 2021;31:8488–97. <https://doi.org/10.1007/s00330-021-07944-4>.
- [11] Haddas R, Ju KL, Belanger T, Lieberman IH. The use of gait analysis in the assessment of patients afflicted with spinal disorders. *Eur Spine J* 2018;27:1712–23. <https://doi.org/10.1007/s00586-018-5569-1>.
- [12] Yoo Y-J, Park J-G, Jo L, Hwang Y, Yoon M-J, Kim J-S, et al. Factors influencing the progression and direction of scoliosis in children with neurological disorders. *Children* 2022;9(1):81.

- [13] Popov I, Lisitsa N, Baloshin Y, Dudin M, Bober S. Variational model of scoliosis. *Theor Appl Mech* 2018;45:167–75. <https://doi.org/10.2298/TAM170818012P>.
- [14] Yilmaz H, Zateri C, Kusvuran Ozkan A, Kayalar G, Berk H. Prevalence of adolescent idiopathic scoliosis in Turkey: an epidemiological study. *Spine J* 2020;20:947–55. <https://doi.org/10.1016/j.spinee.2020.01.008>.
- [15] Motyer GS, Kiely PJ, Fitzgerald A. Adolescents' Experiences of Idiopathic Scoliosis in the Presurgical Period: A Qualitative Study. *J Pediatr Psychol* 2022;47:225–35. <https://doi.org/10.1093/jpepsy/jsab095>.
- [16] Hatzilazaridis I, Hatzitaki V, Antoniadou N, Samoladas E. Postural and muscle responses to galvanic vestibular stimulation reveal a vestibular deficit in adolescents with idiopathic scoliosis. *Eur J Neurosci* 2019;50(10):3614–26. <https://doi.org/10.1111/ejn.14525>.
- [17] Haddas R, Lieberman IH, Kakar RS. A Comparison of muscular activity during gait between walking sticks and a walker in patients with adult degenerative scoliosis. *Spine Deform* 2019;7:454–66. <https://doi.org/10.1016/j.jspd.2018.09.067>.
- [18] Roy S, Grünwald ATD, Alves-Pinto A, Lampe R. Automatic analysis method of 3D images in patients with scoliosis by quantifying asymmetry in transverse contours. *Biocybern Biomed Eng* 2020;40:1486–98. <https://doi.org/10.1016/j.bbe.2020.09.001>.
- [19] Gao C-C, Chern J-S, Chang C-J, Lai P-L, Lung C-W, Tulchin-Francis K. Center of pressure progression patterns during level walking in adolescents with idiopathic scoliosis. *PLoS ONE* 2019;14(4):e0212161. <https://doi.org/10.1371/journal.pone.0212161>.
- [20] Al-Mohrej OA, Aldakhil SS, Al-Rabiah MA, Al-Rabiah AM. Surgical treatment of adolescent idiopathic scoliosis: complications. *Ann Med Surg* 2020;52:19–23. <https://doi.org/10.1016/j.amsu.2020.02.004>.
- [21] Le Berre M, Pradeau C, Brouillard A, Coget M, Massot C, Catanzariti JF. Do adolescents with idiopathic scoliosis have an erroneous perception of the gravitational vertical? *Spine Deform* 2019;7:71–9. <https://doi.org/10.1016/j.jspd.2018.05.004>.
- [22] Tahirbegolli B, Obertinca R, Bytyqi A, Kryeziu B, Hyseni B, Taganoviq B, et al. Factors affecting the prevalence of idiopathic scoliosis among children aged 8–15 years in Prishtina, Kosovo. *Sci Rep* 2021;11:1–7. <https://doi.org/10.1038/s41598-021-96398-1>.
- [23] Zhu F, Hong Q, Guo X, Wang D, Chen J, Zhu Q, Zhang C, Chen W, Zhang M. A comparison of foot posture and walking performance in patients with mild, moderate, and severe adolescent idiopathic scoliosis. *PLoS One* 2021;16:e0251592. <https://doi.org/10.1371/journal.pone.0251592>.
- [24] Peng J. Evaluation of the effectiveness of artificial neural network based on correcting scoliosis and improving spinal health in university students. *J Healthc Eng* 2022;2022:1–9. <https://doi.org/10.1155/2022/2092034>.
- [25] Sklensky J, Urbasek K, Svehlik M, Svozilova V, Kocanda J, Prymek M, et al. The relationship of hip loading asymmetry and radiological parameters of the spine in Lenke type 1 idiopathic scoliosis. *Gait Posture* 2022;94:160–5. <https://doi.org/10.1016/j.gaitpost.2022.03.005>.
- [26] Khorrami Chokami A, Gasparini M, Merletti R. Identification of periodic bursts in surface EMG: Applications to the erector spinae muscles of sitting violin players. *Biomed Signal Process Control* 2021;65:102369. <https://doi.org/10.1016/j.bspc.2020.102369>.
- [27] Garg B, Gupta M, Mehta N, Malhotra R. Influence of etiology and onset of deformity on spatiotemporal, kinematic, kinetic, and electromyography gait variables in patients with scoliosis-a prospective, comparative study. *Spine (Phila Pa 1976)* 2021;46:374–82. <https://doi.org/10.1097/BRS.0000000000003796>.
- [28] Remeseiro B, Bolon-Canedo V. A review of feature selection methods in medical applications. *Comput Biol Med* 2019;112:103375. <https://doi.org/10.1016/j.combiomed.2019.103375>.
- [29] Elsaia WM, Preece SJ, Jones RK, Herrington L. Between-day repeatability of lower limb EMG measurement during running and walking. *J Electromyogr Kinesiol* 2020;55:102473. <https://doi.org/10.1016/j.jelekin.2020.102473>.
- [30] Bains MK. Gait analysis in adolescents with idiopathic scoliosis: A systematic review. 2015.
- [31] Haris M, Chakraborty P, Rao BV. EMG signal based finger movement recognition for prosthetic hand control. In: *Commun. Control Intell. Syst.* IEEE; 2015. p. 194–8. <https://doi.org/10.1109/CCIntels.2015.7437907>.
- [32] Phinyomark A, Phukpattaranont P, Limsakul C. Feature reduction and selection for EMG signal classification. *Expert Syst Appl* 2012;39:7420–31. <https://doi.org/10.1016/j.eswa.2012.01.102>.
- [33] Wu KW, Wang TM, Hu CC, Hong SW, Lee PA, Lu TW. Postural adjustments in adolescent idiopathic thoracic scoliosis during walking. *Gait Posture* 2019;68:423–9. <https://doi.org/10.1016/j.gaitpost.2018.12.024>.
- [34] Jafarnezhadgero AA, Fatollahi A, Amirzadeh N, Siahkouhian M, Granacher U, Mirkov D. Ground reaction forces and muscle activity while walking on sand versus stable ground in individuals with pronated feet compared with healthy controls. *PLoS ONE* 2019;14(9):e0223219. <https://doi.org/10.1371/journal.pone.0223219>.
- [35] Zhou X, Li X, Wu Q, Liang J, Guo H, Jin M, et al. Three-dimensional corrective exercise therapy for idiopathic scoliosis: study protocol for a prospective non-randomized trial. *BMC Musculoskeletal Disord* 2022;23:1–9. <https://doi.org/10.1186/s12891-022-05057-7>.
- [36] Cheung M-C, Yip J, Lai JSK, de Mauroy JC. Biofeedback posture training for adolescents with mild scoliosis. *Biomed Res Int* 2022;2022:1–8. <https://doi.org/10.1155/2022/5918698>.
- [37] Loughenbury PR, Tsirikos AI. Current concepts in the treatment of neuromuscular scoliosis: clinical assessment, treatment options, and surgical outcomes. *Bone Jt Open* 2022;3:85–92. <https://doi.org/10.1302/2633-1462.31.bjo-2021-0178.r1>.
- [38] Park J, So W-Y. The effect of the Schroth rehabilitation exercise program on spinal and feet alignment in adolescent patients with idiopathic scoliosis: A pilot study. *Healthc* 2022;10(2):398.
- [39] Marin I, Lovecchio N, Pedrotti L, Manzoni F, Febbi M, Albanese I, et al. Acute effects of self-correction on spine deviation and balance in adolescent girls with idiopathic scoliosis. *Sensors* 2022;22:1–9. <https://doi.org/10.3390/s22051883>.
- [40] B S, M R, S A, C F. Identification of the most relevant intervertebral effort indicators during gait of adolescents with idiopathic scoliosis. *Comput Methods Biomed Eng* 2020;23(10):664–74. <https://doi.org/10.1080/10255842.2020.1758075>.
- [41] Wick J, Le H, Lafage R, Gupta M, Hart R, Mundis Gregory J, et al., Assessment of adult spinal deformity complication timing and impact on two-year outcomes using a comprehensive adult spinal deformity classification system, *Spine (Phila. Pa. 1976)* 2021. Doi: 10.1097/BRS.0000000000004289.
- [42] Holewijn RM, Kingma I, de Kleuver M, Schimmel JJP, Keijzers NLW. Spinal fusion limits upper body range of motion during gait without inducing compensatory mechanisms in adolescent idiopathic scoliosis patients. *Gait Posture* 2017;57:1–6. <https://doi.org/10.1016/j.gaitpost.2017.05.017>.

- [43] Pesenti S, Prost S, Pomero V, Authier G, Severyns M, Roscigni L, et al. Early dynamic changes within the spine following posterior fusion using hybrid instrumentation in adolescents with idiopathic scoliosis: a gait analysis study. *Arch Orthop Trauma Surg* 2021. <https://doi.org/10.1007/s00402-021-03956-3>.
- [44] Kokabu T, Kanai S, Kawakami N, Uno K, Kotani T, Suzuki T, et al. An algorithm for using deep learning convolutional neural networks with three dimensional depth sensor imaging in scoliosis detection. *Spine J* 2021;21:980–7. <https://doi.org/10.1016/j.spinee.2021.01.022>.
- [45] Wu C, Meng G, Lian J, Xu J, Gao M, Huang C, et al. A multi-stage ensemble network system to diagnose adolescent idiopathic scoliosis. *Eur Radiol* 2022. <https://doi.org/10.1007/s00330-022-08692-9>.
- [46] Caesarendra W, Rahmaniar W, Mathew J, Thien A. Automated Cobb angle measurement for adolescent idiopathic scoliosis using convolutional neural network. *Diagnostics* 2022;12:396.
- [47] Li J, Li S, Yang Z, Wu T, Hu Y. An automatic scoliosis diagnosis platform based on deep learning approach. *ACM Int Conf Proceeding Ser* 2022:215–23. <https://doi.org/10.1145/3512353.3512385>.
- [48] Holewijn R, Kingma I, de Kleuver M, Schimmel J, Keijsers N, Near preoperative shoulder and trunk range of motion during gait after surgical correction of adolescent idiopathic scoliosis, *Glob Spine J.* 2016;6. Doi: 10.1055/s-0036-1582682.
- [49] Syczewska M, Kocel K, Święcicka A, Graff K, Krawczyk M, Wąsiewicz P, et al. Selection of gait parameters for modified Gillette Gait Index using Hellwig Correlation Based Filter method, random forest method, and correlation methods. *Biocybern Biomed Eng* 2020;40:1267–76. <https://doi.org/10.1016/j.bbe.2020.07.002>.